CHAPTER 6 – ANALYTIC MODEL OF ULTRASONIC SCATTERING BY A CYLINDRICAL HOLE WITH AN ELASTIC ANNULUS

6.1 Background

A factor that may affect the performance of the proposed ultrasonic inspection approach is the existence of a polyurathane coating on the inside surface of the weep hole. This coating is used to protect the surface of the hole from corrosion. The thickness of the layer is approximately 0.002 in. ($h/\lambda \cong 0.1$). The weep hole top crack detection procedure has been shown to be sensitive down to 0.002 in. ($l/\lambda \cong 0.1$) thus on the same order as the thickness of the elastic layer [16]. Therefore, the characteristics of a coating may significantly change the nature of the 'leaky' Rayleigh wave as it propagates about the weep hole. The current procedure requires that the coating be removed prior to inspection. A significant reduction in time and effort would be gained by eliminating the need for the removal of this coating. The development of a model would produce the needed understanding in order to assess the viability of using the 'leaky' Rayleigh wave procedure for radial fatigue crack detection for this case.

Guided waves in a single axisymmetric domain have been extensively examined. The analytic derivation for the propagation of Rayleigh waves on a cylindrical surface was presented by Viktorov and others [56,57,47]. Unlike Rayleigh waves on an elastic

half-space, these waves are dispersive. The dispersion relation has also been derived for the case of an elastic annulus [58]. As for the cylindrical surface case, the guided waves within the annulus are dispersive. The first mode for this case was determined to be a Rayleigh-type mode. For a thick annulus (where the ratio of the annulus thickness, h, to the annulus outer diameter, b, is equal to 0.90), the Rayleigh-type mode is found on the inner annulus surface, while for a thin annulus (h / b = 0.05), the Rayleigh-type mode is localized predominantly on the outer annulus surface [59].

The study of wave propagation in an elastic layer bounded by a second medium has a significant history. At the bond between two elastic half-spaces with different elastic properties, under certain conditions Stoneley waves can be found to propagate along the interface [60]. Free harmonic waves for a layer in smooth and bonded contact with an elastic half-space were investigated by Achenbach and Epstein [61]. It was shown that when the wavelength is small (or the layer is thin), only one mode of propagation exists close to the surface whose phase velocity is very close to the Rayleigh wave velocity for a half-space. The effect of curvature on Stoneley waves was investigated by Epstein [62] who considered an infinite elastic domain with a cylindrical elastic inclusion of different material properties.

A body of work has investigated the interaction of an elastic layer with a circular cylinder. Wave propagation in composite cylinders was initially investigated by Epstein [63]. The composite cylinder is defined as an elastic cylinder encased by a second elastic cylinder. Epstein examined the phase velocity for the lowest modes of propagation for bonded and smooth contact conditions based on the derived dispersion relations. Valle et

al. numerically solved the dispersion relation for the case of a layered cylinder with an interface of smooth contact [64]. Additional works have investigated wave propagation in composite cylinders for the detection of the characteristics of the surface layer [65] and for the determination of the existence of surface breaking cracks radiating outward from the boundary between the two cylinders [66]. Within the large body of work on fiber-matrix composites, the special case of a cylindrical fiber with an interphase elastic coating embedded in an elastic matrix has been examined [67,68]. Sinclair and Addison investigated normal incidence of compressional waves for this case [67]. Rokhlin et al examined the scattering model for the case of a core with multiple interphase layers embedded in an elastic medium [68].

Our problem of interest is the reverse of these cases where a hollow elastic cylinder is bonded inside an infinite elastic medium. Pao and Mow investigated the cavity in an infinite elastic medium with an elastic liner for the case of an incident plane longitudinal wave [52]. The primary focus of their work was to understand the effect of an elastic liner on stress concentrations around the cavity.

In this study, the dispersion relation will be first derived. Numerical solutions for the phase velocity and the attenuation of the lowest modes will be obtained and examined. The analytic solution of the scattering response to an incident shear plane wave by a cylindrical hole with an elastic coating will be derived. Parametric studies will be performed to understand the sensitivity of the 'leaky' Rayleigh wave to variation of the geometric and material properties of the annulus. With these results, an estimate of

the sensitivity of the inspection procedure to the properties of the elastic annulus will be made.

6.2 Derivation of Dispersion Relation

Figure 6.1 displays an elastic annulus embedded in an infinite elastic medium. The subscript 1 is given to the material properties for the annulus region. The approach for the development of the dispersion relation will be similar to the approach used by Epstein [63].

The general solution for the scalar and vector potentials for two dimensional plane strain elasticity in terms of cylindrical coordinates are given by

$$\boldsymbol{j}_1(r,\boldsymbol{q},t) = \left\{A\left[J_n(\boldsymbol{a}_1 kr)\right] + B\left[Y_n(\boldsymbol{a}_1 kr)\right]\right\} e^{-iwt} \sin n\boldsymbol{q}\,, \tag{6.1}$$

$$\boldsymbol{y}_{z1}(r,\boldsymbol{q},t) = \left\{C\left[J_n(\boldsymbol{b}_1 kr)\right] + D\left[Y_n(\boldsymbol{b}_1 kr)\right]\right\} e^{-iwt} \cos n\boldsymbol{q}\,, \tag{6.2}$$

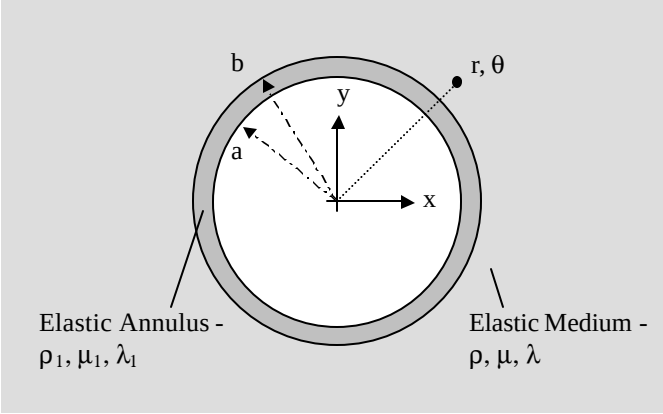

Figure 6.1. Elastic annulus bonded to a cylindrical cavity in an infinite elastic medium.

where:

$$k = \frac{\omega}{c}, \quad \alpha_1 = \frac{c}{c_L}, \quad \beta_1 = \frac{c}{c_T}.$$

These solutions can be used in the equations for the displacements, u_r and u_θ, and the stresses, τ_r and $\tau_{r\theta}$, given respectively by

$$u_r = \frac{\partial \phi}{\partial r} + \frac{1}{r}\frac{\partial \psi_z}{\partial \theta}, \tag{6.3}$$

$$u_\theta = \frac{1}{r}\frac{\partial \phi}{\partial \theta} - \frac{\partial \psi_z}{\partial r}, \tag{6.4}$$

$$\tau_r = \lambda\left(\frac{\partial u_r}{\partial r} + \frac{u_r}{r} + \frac{1}{r}\frac{\partial u_\theta}{\partial \theta}\right) + 2\mu\frac{\partial u_r}{\partial r}, \tag{6.5}$$

$$\tau_{r\theta} = \mu\left(\frac{\partial u_\theta}{\partial r} - \frac{u_\theta}{r} + \frac{1}{r}\frac{\partial u_r}{\partial \theta}\right). \tag{6.6}$$

Expressions for the general solutions for displacements and stresses in cylindrical coordinates for the annular region are thus given by

$$u_{r1} = \left\{\begin{array}{l} A\left[-\frac{n}{r}J_n(\alpha_1 kr) + \alpha_1 k J_{n-1}(\alpha_1 kr)\right] \\ + B\left[-\frac{n}{r}Y_n(\alpha_1 kr) + \alpha_1 k Y_{n-1}(\alpha_1 kr)\right] \\ - C\left[\frac{n}{r}J_n(\beta_1 kr)\right] - D\left[\frac{n}{r}Y_n(\beta_1 kr)\right] \end{array}\right\} e^{-i\omega t} \sin n\theta, \tag{6.7}$$

$$u_{q1}=\left\{\begin{array}{l}A\left[\frac{n}{r}J_n(\boldsymbol{a}_1kr)\right]+B\left[\frac{n}{r}Y_n(\boldsymbol{a}_1kr)\right]\\+C\left[\frac{n}{r}J_n(\boldsymbol{b}_1kr)-\boldsymbol{b}_1kJ_{n-1}(\boldsymbol{b}_1kr)\right]\\+D\left[\frac{n}{r}Y_n(\boldsymbol{b}_1kr)-\boldsymbol{b}_1kY_{n-1}(\boldsymbol{b}_1kr)\right]\end{array}\right\}\mathrm{e}^{-iwt}\cos n\boldsymbol{q}\,, \tag{6.8}$$

$$\boldsymbol{t}_{r1}=2\boldsymbol{m}_1\left\{\begin{array}{l}A\left[\left(\frac{n^2+n}{r^2}-\frac{1-\boldsymbol{n}_1}{1-2\boldsymbol{n}_1}(\boldsymbol{a}_1k)^2\right)J_n(\boldsymbol{a}_1kr)-\frac{\boldsymbol{a}_1k}{r}J_{n-1}(\boldsymbol{a}_1kr)\right]\\+B\left[\left(\frac{n^2+n}{r^2}-\frac{1-\boldsymbol{n}_1}{1-2\boldsymbol{n}_1}(\boldsymbol{a}_1k)^2\right)Y_n(\boldsymbol{a}_1kr)-\frac{\boldsymbol{a}_1k}{r}Y_{n-1}(\boldsymbol{a}_1kr)\right]\\-C\left(\frac{n}{r}\right)\left[\left(-\frac{n+1}{r}\right)J_n(\boldsymbol{b}_1kr)+\boldsymbol{b}_1kJ_{n-1}(\boldsymbol{b}_1kr)\right]\\-D\left(\frac{n}{r}\right)\left[\left(-\frac{n+1}{r}\right)Y_n(\boldsymbol{b}_1kr)+\boldsymbol{b}_1kY_{n-1}(\boldsymbol{b}_1kr)\right]\end{array}\right\}\mathrm{e}^{-iwt}\sin n\boldsymbol{q}\,,$$

(6.9)

$$\boldsymbol{t}_{rq1}=2\boldsymbol{m}_1\left\{\begin{array}{l}A\left(\frac{n}{r}\right)\left[\left(-\frac{n+1}{r}\right)J_n(\boldsymbol{a}_1kr)+\boldsymbol{a}_1kJ_{n-1}(\boldsymbol{a}_1kr)\right]\\+B\left(\frac{n}{r}\right)\left[\left(-\frac{n+1}{r}\right)K_n(\boldsymbol{a}_1kr)+\boldsymbol{a}_1kK_{n-1}(\boldsymbol{a}_1kr)\right]\\-C\left[\left(\frac{n^2+n}{r^2}-\frac{1}{2}(\boldsymbol{b}_1k)^2\right)J_n(\boldsymbol{b}_1kr)-\frac{\boldsymbol{b}_1k}{r}J_{n-1}(\boldsymbol{b}_1kr)\right]\\-D\left[\left(\frac{n^2+n}{r^2}-\frac{1}{2}(\boldsymbol{b}_1k)^2\right)K_n(\boldsymbol{b}_1kr)-\frac{\boldsymbol{b}_1k}{r}K_{n-1}(\boldsymbol{b}_1kr)\right]\end{array}\right\}\mathrm{e}^{-iwt}\cos n\boldsymbol{q}\,.$$

(6.10)

Due to the radiation condition for the infinite elastic medium, the general solutions for the scalar and vector potentials are given by

$$\boldsymbol{j}(r,\boldsymbol{q},t)=\left\{E\left[H_n^{(1)}(\boldsymbol{a}kr)\right]\right\}\mathrm{e}^{-iwt}\sin n\boldsymbol{q}\,, \tag{6.11}$$

$$\psi_z(r,\theta,t) = \left\{F\left[H_n^{(1)}(\beta kr)\right]\right\} e^{-i\omega t} \cos n\theta . \tag{6.12}$$

It can then be shown that the general solutions for the displacements and stresses in the infinite elastic region are given by

$$u_{r2} = \left\{E\left[-\frac{n}{r}H_n^{(1)}(\alpha kr) + \alpha k H_{n-1}^{(1)}(\alpha kr)\right] - F\left[\frac{n}{r}H_n^{(1)}(\beta kr)\right]\right\} e^{-i\omega t} \sin m\theta , \tag{6.13}$$

$$u_{\theta 2} = \left\{E\left[\frac{n}{r}H_n^{(1)}(\alpha kr)\right] + F\left[\frac{n}{r}H_n^{(1)}(\beta kr) - \beta k H_{n-1}^{(1)}(\beta kr)\right]\right\} e^{-i\omega t} \cos m\theta , \tag{6.14}$$

$$\tau_{r2} = 2\mu \left\{\begin{array}{l} E\left[\left(\frac{n^2+n}{r^2} - \frac{1-\nu}{1-2\nu}(\alpha k)^2\right)H_n^{(1)}(\alpha kr) - \frac{\alpha k}{r}H_{n-1}^{(1)}(\alpha kr)\right] \\ -F\left(\frac{n}{r}\right)\left[\left(-\frac{n+1}{r}\right)H_n^{(1)}(\beta kr) + \beta k H_{n-1}^{(1)}(\beta kr)\right] \end{array}\right\} e^{-i\omega t} \sin m\theta , \tag{6.15}$$

$$\tau_{r\theta 2} = 2\mu \left\{\begin{array}{l} E\left(\frac{n}{r}\right)\left[\left(-\frac{n+1}{r}\right)H_n^{(1)}(\alpha kr) + \alpha k H_{n-1}^{(1)}(\alpha kr)\right] \\ -F\left[\left(\frac{n^2+n}{r^2} - \frac{1}{2}(\beta k)^2\right)H_n^{(1)}(\beta kr) - \frac{\beta k}{r}H_{n-1}^{(1)}(\beta kr)\right] \end{array}\right\} e^{-i\omega t} \cos m\theta . \tag{6.16}$$

The boundary conditions at r = a are, $\tau_{r1}(a,\theta,t) = 0$, $\tau_{r\theta 1}(a,\theta,t) = 0$, and the interface conditions at r = b state that, $u_{r1}(b,\theta,t) = u_{r2}(b,\theta,t)$, $u_{\theta 1}(b,\theta,t) = u_{\theta 2}(b,\theta,t)$, $\tau_{r1}(b,\theta,t) = \tau_{r2}(b,\theta,t)$, $\tau_{r\theta 1}(b,\theta,t) = \tau_{r\theta 2}(b,\theta,t)$. For the interface conditions of continuous stresses and displacements to be met, the angular wave numbers *n* and *m* must be equal. Also, to insure continuity at the interface, it follows that $n = m = kb$. After application of the interface conditions and with some manipulation, the homogeneous system of equations can be expressed as

$$[\mathbf{M}]\,\mathbf{X} = 0, \tag{6.17}$$

where $\mathbf{X}=[A, B, C, D, E, F]^T$. The 6×6 matrix [**M**] is presented in Appendix B. For non-trivial solutions, the dispersion relation can be expressed in terms of the matrix **M** whose determinant is set to zero, where

$$\text{Det } [\mathbf{M}] = 0. \tag{6.18}$$

Within the 6×6 matrix [**M**], a 2×2 matrix, [**M**(3..4,5..6)], representing the dispersion relation for a cylindrical hole in an infinite elastic medium as derived by Viktorov [56,57] is shown. Also, a 4×4 matrix, [**M**(1..4,1..4)], representing the dispersion relation for an elastic annulus as derived by Qu et al [58,59] can be found. The dispersion relation derived by Epstein for the case of a hollow cylinder bonded to a second cylinder can be obtained from this equation by swapping *a* for *b* in the parameters *n* and *g*, and by replacing the Hankel function, $H_n^{(1)}(z)$, with Bessel function, $J_n(z)$, in columns 5 and 6 of matrix [**M**] [63].

6.3 Numerical Solution of Dispersion Relation

In order to solve the dispersion relation, complex angular wave numbers (of the form $n = n_r + i \cdot n_i$) are necessary. The imaginary part of the angular wave number corresponds to attenuation of the mode, which is expected for modes in an infinite elastic domain. Thus, the Bessel and Hankel functions must be evaluated for both complex order and argument. Numerical strategies have been developed to evaluate Bessel and Hankel functions for certain ranges of complex order and argument [69,70]. A program

was written in Maple, which incorporates these numerical strategies, to search for complex roots in *n* representing the lowest modes of interest. A search algorithm was implemented which performed an initial exhaustive search, located regions of zeros within the search domain and refined the root solutions using the bisection method [71,72]. These roots were calculated for a selected range of frequencies corresponding to the inspection problem. With each solution for the complex angular wave number, the phase velocity and the attenuation coefficient of the circumferential mode can be calculated. The phase velocity and attenuation are given by the following relations:

$$c_p(\omega) = \frac{b\omega}{\mathrm{Re}(n(\omega))}, \tag{6.19}$$

$$\alpha(\omega) = \frac{\mathrm{Im}(n(\omega))}{b}. \tag{6.20}$$

Hassan and Nagy used this analysis approach for the fluid-filled cavity case [18].

The material properties of aluminum were used for the infinite elastic medium (see Appendix A). The properties of urethane polymers were found to exhibit some variability. The density may vary between 1.0 to 1.2 g/cm^3 and longitudinal wave speeds (measured at 1 MHz) may range from 1500 to 1800 m/s [73]. For the purpose of a parameter study in an upcoming section and for simplicity, a single material non-dimensional parameter, ζ, will be defined where the density and the wave speeds for the layer are given by the following relations:

$$\rho_1 = \zeta \times \rho, \tag{6.21}$$

$$c_{1,L} = \zeta \times c_L, \tag{6.22}$$

$$c_{1,T} = \zeta \times c_T. \tag{6.23}$$

Values of ζ as 0 and 1 represent 'no layer', and 'the layer being of the same material' (i.e. smaller hole diameter) respectively. A value of $\zeta = 0.5$ was used as a rough approximation of a urethane polymer layer for the numerical solution of the dispersion relation.

Figure 6.2 displays the dispersion curves where the phase velocity of the circumferential mode normalized with respect to the shear wave velocity of the elastic layer ($c_p / c_{1,T}$) is plotted with respect to the normalized frequency ($W = \omega \times b / c_T$, where b is the outer diameter of the annulus). The two lowest circumferential modes for the cylindrical cavity with an elastic insert are compared with the dispersion curves for the cylindrical cavity, and for the elastic annulus. The geometric parameter, h/b, was set to 0.05 and the material non-dimensional parameter was set to 0.5. These parameter settings represent a layer somewhat thicker and stiffer than what is found in the field. Of particular interest, the corresponding normalized frequency for an ultrasonic transducer center frequency of 5.0 MHz for the weep hole inspection case is 31.9.

At lower frequencies, the first circumferential mode equates well with the dispersion curve for the cylindrical hole case. Clearly, when the wavelength of the circumferential mode is large, the relative thickness of the layer is small, and thus has little impact on the response. Therefore, very thin layers composed of a softer material ($\zeta = 0.5$) produce little change in the 'leaky' Rayleigh wave for the empty cylindrical hole case.

As the frequency is increased, the first circumferential mode decreases in phase velocity and shifts toward the lowest mode of the elastic annulus case. Likewise for the second circumferential mode, a decrease in the phase velocity is observed approaching the second lowest mode for the elastic annulus case. At the center frequency of the inspection transducer, the existence of the layer produces a significant difference in the phase velocity with respect to the empty cylindrical hole case. Clearly, a measurable change in the 'leaky' Rayleigh wave is expected for the selected layer parameters. Due to the thickness of the layer being relatively thin, only a few modes are observed within the range of frequencies and phase velocities solved. A significant increase in the thickness of the layer would further impact the circumferential modes.

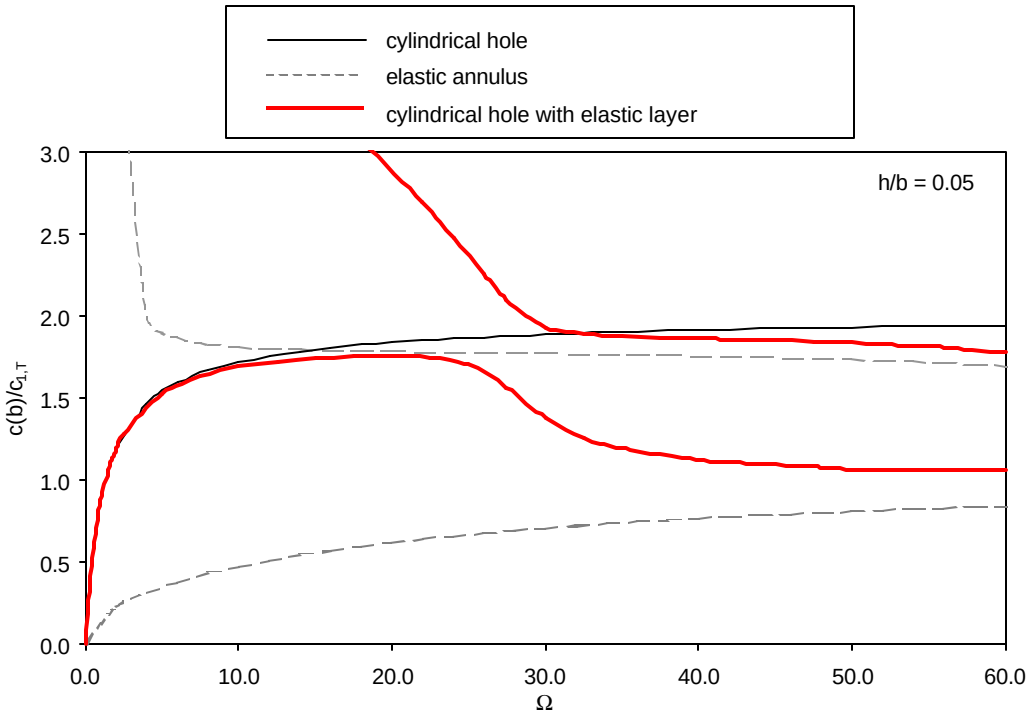

Figure 6.2. Dispersion curves for circumferential wave propagating around a cylindrical cavity with an elastic layer, a cylindrical cavity, and an elastic annulus.

Figure 6.3 displays the normalized attenuation of the circumferential mode plotted with respect to normalized frequency. The lowest circumferential mode for the cylindrical cavity with an elastic insert case is compared with the cylindrical cavity result over a limited frequency range. Clearly, the attenuation of the first mode for the cylindrical cavity with an elastic insert is reduced significantly with respect to the cylindrical hole case. This reduction in attenuation is contributed to loss of the 'leaky' Rayleigh wave into the elastic layer.

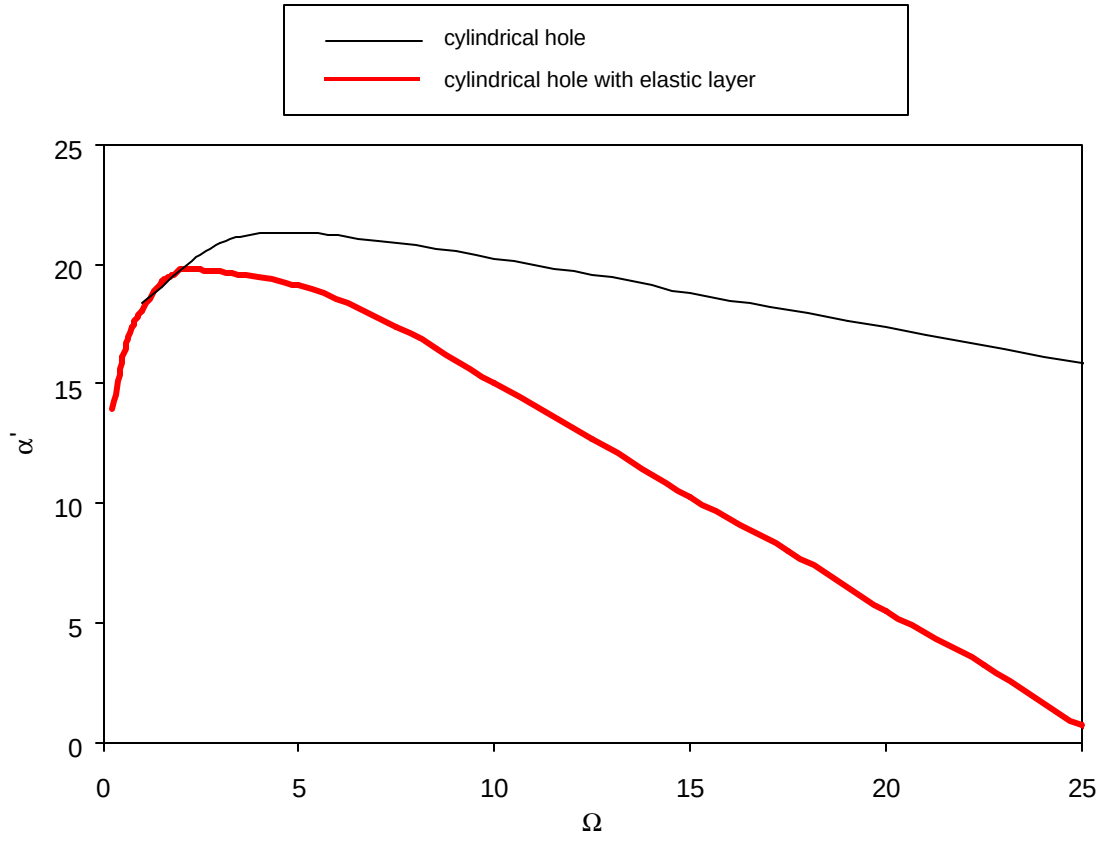

Figure 6.3. Attenuation curves for circumferential wave propagating about a cylindrical cavity with an elastic layer, and a cylindrical cavity.

6.4 Analytic Response to Incident Plane Shear Wave

An extension of this analytical derivation may be performed by deriving the transient scattering response due to a plane shear wave incident on a cavity with an elastic layer. Pao and Mow previously investigated the case of a cavity in an infinite elastic medium with an elastic liner for an incident plane longitudinal wave [52]. For the present study, the case of an incident plane shear wave will be solved. To obtain the transient response, a transient pulse is first defined in the frequency domain, the expansion coefficients are solved for a selected range of frequencies, and the inverse Fourier transform is applied to calculate the solution for the locations of interest. Hassan and Nagy [20] used this transient analysis approach to better understand the nature of the 'leaky' Rayleigh wave for the fluid-filled weep hole case.

The general solution for the scalar and vector potentials for an incident plane shear wave in terms of cylindrical coordinates are given by

$$\boldsymbol{j}_i(r,\boldsymbol{q},t) = 0, \tag{6.24}$$

$$\boldsymbol{y}_i(r,\boldsymbol{q},t) = \boldsymbol{y}_0 \sum_{n=0}^{\infty} \boldsymbol{e}_n i^n \left[J_n(\boldsymbol{b}kr)\right] \mathrm{e}^{-i\boldsymbol{w}t} \cos n\boldsymbol{q}. \tag{6.25}$$

where $\boldsymbol{e}$ is the Neumann factor such that $\boldsymbol{e}_0 = 1$, $\boldsymbol{e}_n = 2$ ($n \geq 1$) [50]. Clearly, the incident displacements and tractions can be solved, and subsequently, the traction free boundary conditions at r = a, and the continuity interface conditions at r = b can be written. The system of equations can be expressed as

$$[\mathbf{M}]\,\mathbf{X} = y_0\,\mathbf{I}\,, \tag{6.26}$$

where $\mathbf{X}=[A, B, C, D, E, F]^T$ and $\mathbf{I}$ are known. For each frequency, the six expansion coefficients can be solved for N number of angular wave numbers in order to properly reconstruct the response. The value of N is determine through verification of convergence for each frequency. The incident wave signal and the corresponding frequency spectrum that were used to represent a typical inspection transducer are shown in Figures 4.5(a) and 4.5(b) respectively.

Figures 6.4 and 6.5 display the transient in-plane deflection amplitude for a cylindrical hole with an elastic layer for widths of h/b = 0.02 and 0.05 respectively. The response was calculated at 19 locations where r = 3 b and θ was varied between 0° and 180° by increments of 10°. Larger incident and specular signals were truncated in order to clearly show the features of the 'leaky' Rayleigh wave.

For the case of h/b = 0.02 shown in Figure 6.4, following the incident signal and the specular reflection response, the 'leaky' Rayleigh wave response is shown. This 'leaky' Rayleigh wave response is quite similar to the previously observed response for the empty hole case. For the case of h/b = 0.05 shown in Figure 6.5, more significant deviation of the 'leaky' Rayleigh wave response from the empty hole case is observed. As the width of the layer is increased, an increased interaction of the 'leaky' Rayleigh wave with the elastic layer is observed. The observed spreading of the 'leaky' Rayleigh wave due to loss into the layer and subsequent re-radiation from the layer corresponds with the dispersions curve results shown in Figure 6.2.

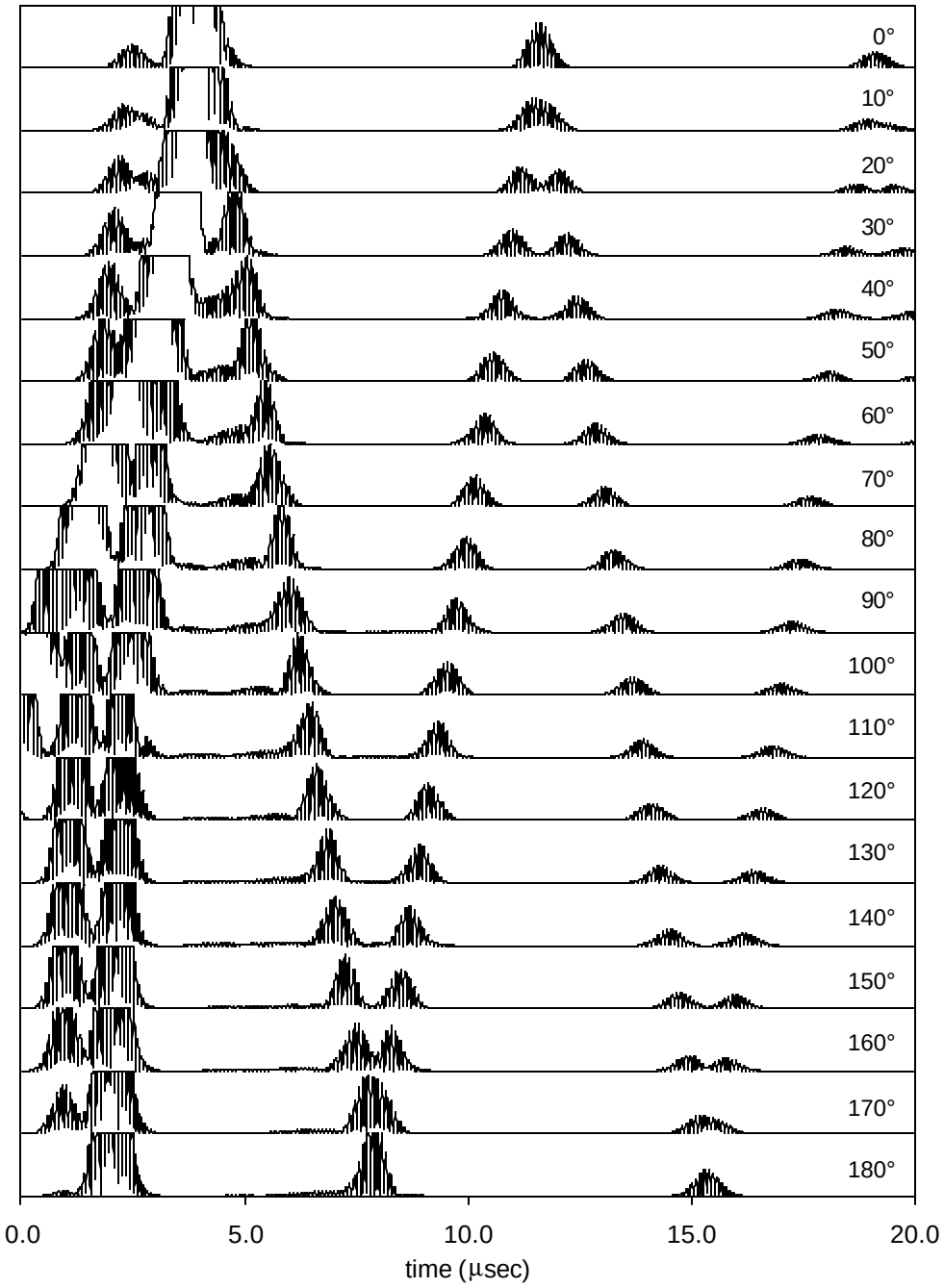

Figure 6.4. Response to incident shear plane wave at locations r=3 b for h/b = 0.02.

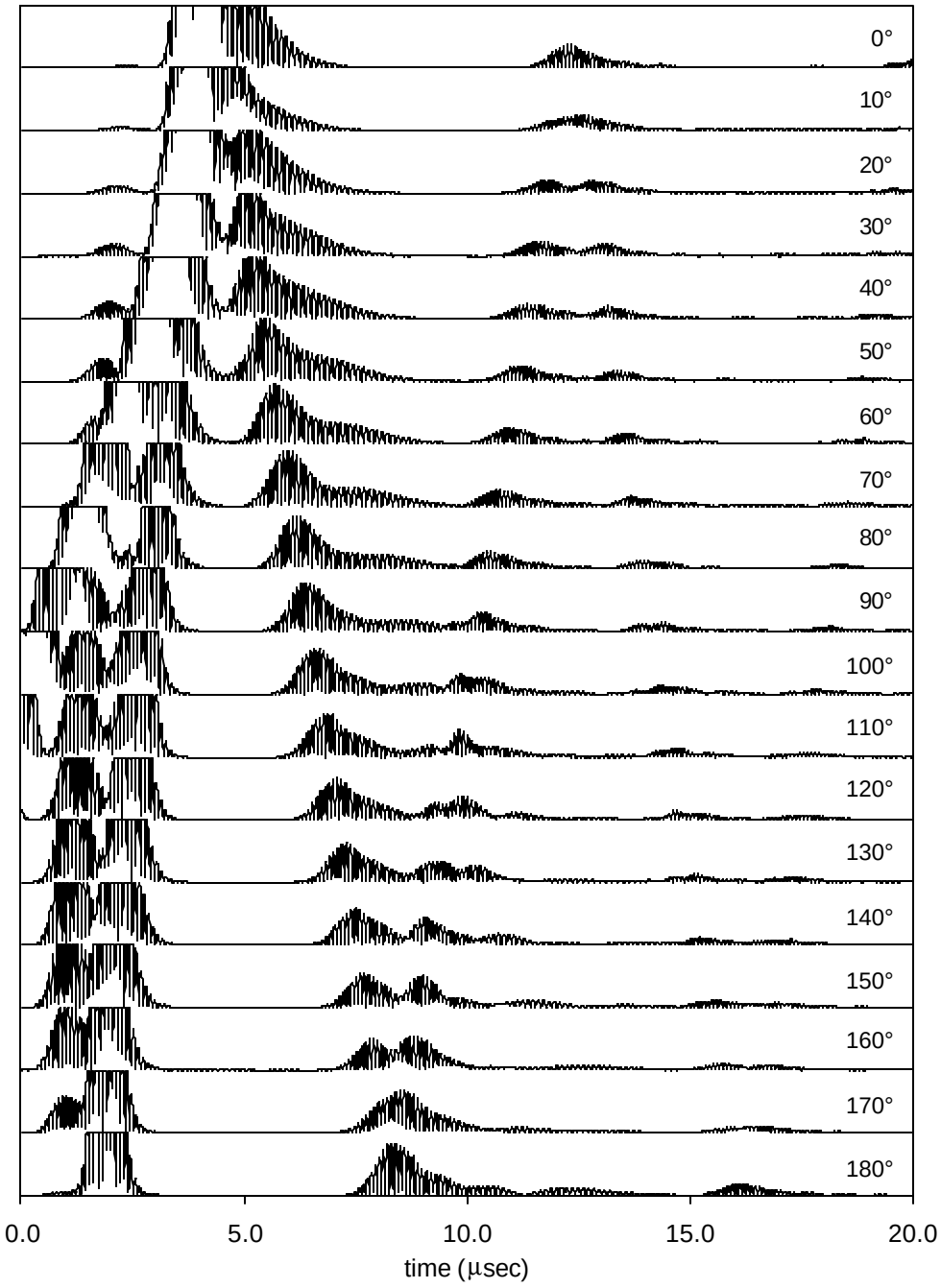

Figure 6.5. Response to incident shear plane wave at locations r=3 b for h/b = 0.05.

Two parameter studies were performed using this transient analytic model. The effect of variation in the thickness of the elastic annulus was first examined. Figure 6.6 displays the transient in-plane deflection amplitude at r = 3 b, θ =180°, for a cylindrical hole with an elastic layer where h/b was varied from 0.00 to 0.20 and ζ set to 0.50. This choice of location corresponds to an approximate location of a measurement transducer. First, with an increase in the width of the elastic layer, the time of flight of the 'leaky' Rayleigh wave increases. This can be correlated to a decrease in the phase velocity of the 'leaky' Rayleigh wave as observed in the dispersion relation shown in Figure 6.2. In addition, as the layer width is increased, loss into the layer and subsequent re-radiation from the layer produces the observed spreading of the 'leaky' Rayleigh wave signal. In terms of the dispersion relation, the higher circumferential modes contribute more greatly to the response as the layer thickness is increased.

The effect of variation in the material non-dimensional parameter, ζ, was also examined. Figure 6.7 displays the transient in-plane deflection amplitude at r = 3 b, θ =180°, for a cylindrical hole with an elastic layer where ζ was varied from 0.0 to 1.0 and h/b was set to 0.05. For ζ = 0.0, the empty cylindrical hole response was recovered. For ζ = 1.0, the layer is of the same material which results in the diameter of the hole being reduce by 5%. As expected for the ζ = 1.0 case, a reduction of the time of flight by 5% is observed. As ζ is increased from 0.0, there is an increase in the time of flight of the 'leaky' Rayleigh wave, followed by a subsequent reduction in the time of flight as ζ as

approaches 1.0. For $\zeta = 0.167$, a resonance of the incident signal with the elastic layer is observed.

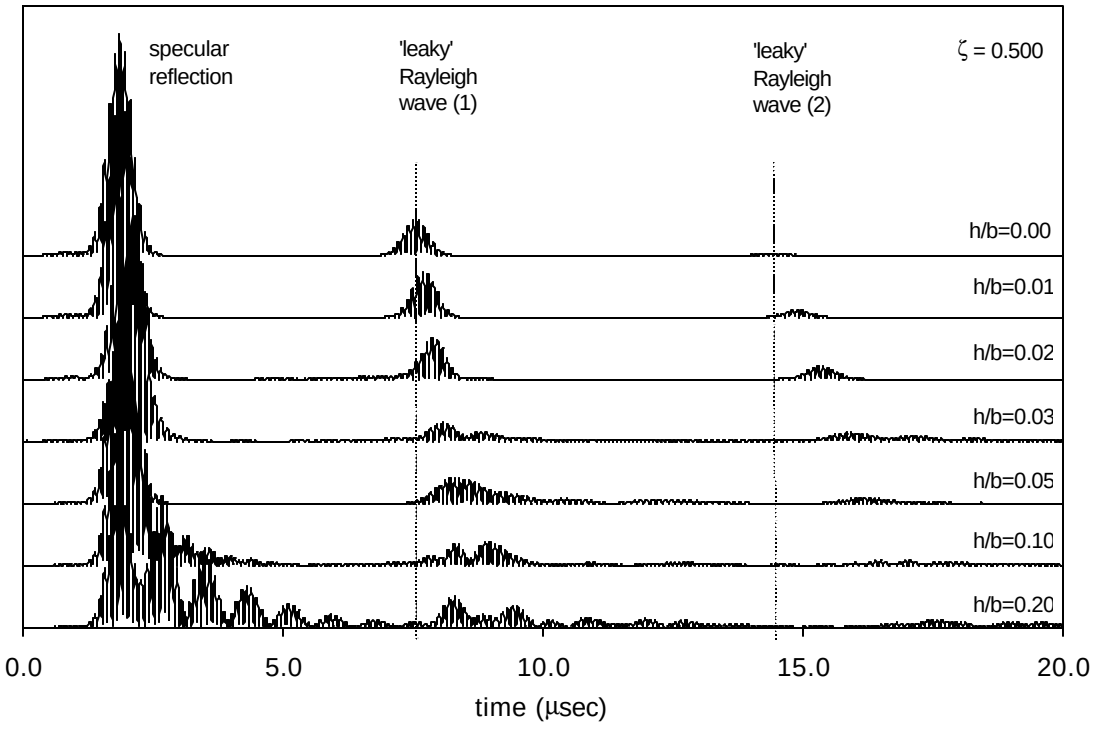

Figure 6.6. Response to incident shear plane wave at location r=3 b, $\theta = 0°$ for various layer geometric parameter settings (h/b).

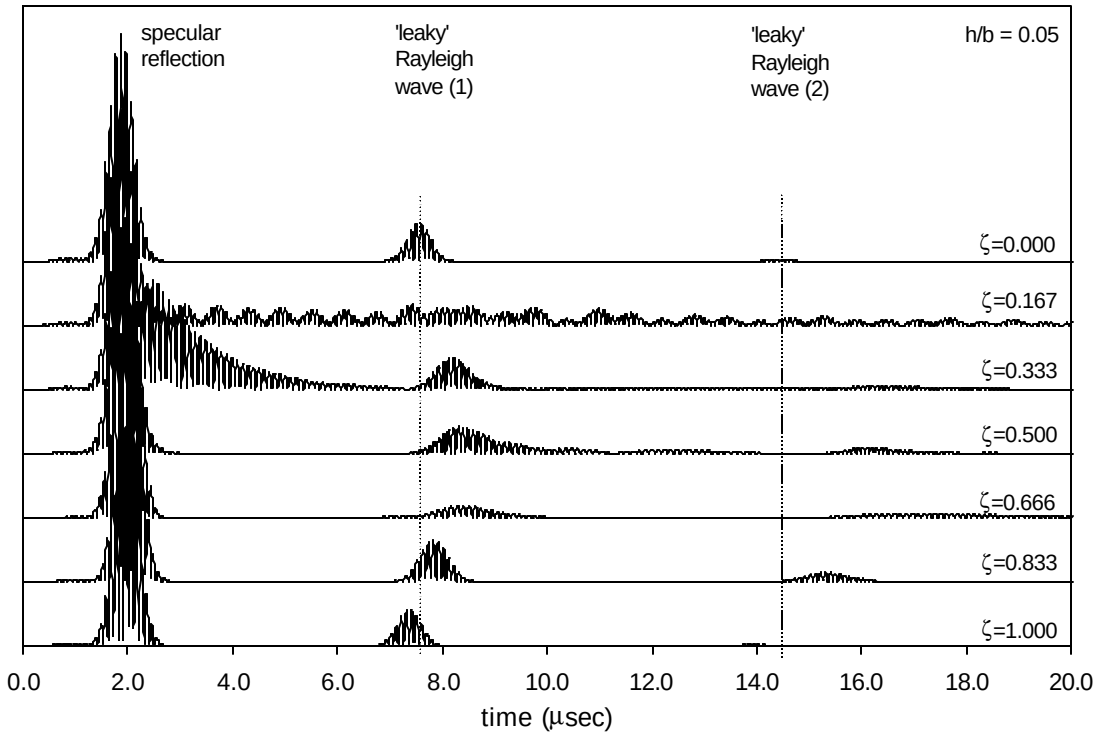

Figure 6.7. Response to incident shear plane wave at location r=3 b, $\theta = 0°$ for various material non-dimensional parameter settings (ζ from 0.0 to 1.0).

6.5 Discussion

Through these studies, a better understanding into the effect of an elastic layer on the propagation of a 'leaky' Rayleigh wave about a cylindrical hole was gained. From an inspection perspective, a small time of flight increase in the measurement of the 'leaky' Rayleigh wave was observed. In addition, as the elastic layer is increased in thickness, loss into the layer and subsequent reradiation from the layer resulting in 'spreading' of the measurement signal is observed. For the range of the polyurethane coating thicknesses expected in the field, this amount of signal variation will have little impact on the peak-to-peak measurement performed for top crack detection. However, this signal variation would produce a major challenge for accurately performing top crack sizing.